ELSEVIER

Fusion Engineering and Design 32–33 (1996) 209–217

Fusion Engineering and Design

Emittance growth from merging arrays of round beamlets

O.A. Anderson[1]

Lawrence Berkeley National Laboratory, 1 Cyclotron Road, Berkeley, CA 94720, USA

Abstract

The cost of an induction linac for heavy ion fusion (HIF) may be reduced if the number of channels in the main accelerator is reduced. There have been proposals to do this by merging beamlets (perhaps in groups of four) after a suitable degree of preacceleration. This process, which results in r.m.s. emittance growth, occurs in two stages.

The first stage occurs instantly when the beamlets, no longer separated by electrodes, enter the merging region. At this point one has a *collection* of beamlets whose centers are displaced from the central axis by distances δ_{xi}, δ_{yi}. The mean square emittance, now calculated for the whole collection, is $\epsilon_{xi}^2 = \epsilon_{x1}^2 + \langle \delta_x^2 \rangle V_x^2$ and similarly for the y direction. Here ϵ_{x1} is the emittance of one undisplaced beamlet, V_x is the r.m.s. thermal velocity and ϵ_{xi} is the *initial* emittance of the *composite* beam. This first stage of emittance growth is easy to calculate and has obvious scaling properties.

The second stage of merged beam emittance growth mostly occurs in about one-quarter of a plasma period, although the full development may take much longer. In this stage, space charge forces cause transverse accelerations. The maximum increase in mean square emittance is proportional to the excess electrostatic energy (free energy) in the array when the merging begins. It tends to dominate the first stage for strongly depressed initial tunes. The relatively complex calculations involving the second stage are the main concern of this paper.

In some designs it may be desirable to reduce the emittance growth below that produced by a basic 2×2 array. For this a general understanding of the free energy is helpful. Therefore we investigate three factors affecting the normalized free energy U_n of an array of charged interacting beamlets: (1) the number of beamlets N in the array; (2) the ratio η of beamlet diameter to beamlet center spacing; (3) the shape of the array. For circular arrays we obtain an analytic expression for U_n as a function of N and η. If η is held constant, it shows that $U_n \sim N^{-1}$ in the large-N limit, i.e. U_n would become arbitrarily small in this idealized case. We show that this is not true for square or rectangular arrays, which have larger free energy with a lower limit determined by the non-circular format. Free energy in square arrays can be reduced by omitting corner beamlets; in the case of a 5×5 array the reduction factor is as large as 3.3.

1. Introduction

Free space charge field energy leads to emittance growth, a fact known since the pioneering analysis by Lapostolle [1] and utilized by Lee et al. [2] in another early contribution. Free energy exists if the initial charge distrubution is non-uniform, which is always the case for merging beamlets. Celata et al. [3] analyzed the free energy of a system of four beamlets located symmetrically within a conducting pipe. More recently, Lee [4]

[1] Also affiliated with Particle Beam Consultants, 2910 Benvenue Avenue, Berkeley, CA 94705, USA.

PII S0920-3796(96)00471-1

analyzed the general case of N non-overlapping round beamlets with arbitrary radii, currents and positions. He also obtained an approximation for the case where the conducting pipe is several times larger than the array of N beamlets. With the beamlet radii a_i, charges per unit length λ_1, positions $\boldsymbol{\delta}_i$ and array center of mass $\boldsymbol{\delta}_c \equiv (\Sigma_i \lambda_i)^{-1} \Sigma_i \lambda_i \boldsymbol{\delta}_i$, Lee wrote a_T^2 (twice the mean square radius of the total array) as

$$a_T^2 = \left(\sum_i \lambda_i\right)^{-1} \sum_i [\lambda_i (a_i^2 + 2\delta_i^2 - 2\delta_c^2)] \tag{1}$$

and found free energy

$$U_f = \frac{1}{4\pi\varepsilon_0}\left\{\sum_i \lambda_i^2 \ln\left(\frac{a_T}{a_i}\right) - \sum_j \sum_{i<j} \lambda_i \lambda_j \left[\frac{1}{2} + \ln\left(\frac{|\boldsymbol{\delta}_i - \boldsymbol{\delta}_j|^2}{a_T^2}\right)\right]\right\} \tag{2}$$

U_f is the difference between the initial field energy and the field energy of a single uniform beam with the same total current and mean square radius.

We make further analytical progress in Section 2 by specializing Lee's result to the case of identical beamlets all with the same current and radius. This simplification leads to a clear understanding of how the final emittance depends on the initial beam parameters.

Section 3 analyzes the case of circular arrays, proposed for magnetic fusion injectors [5]. We show that the normalized free energy $U_n \to 4N^{-1}[\frac{3}{4} - \ln(3\eta) + \frac{3}{8}\eta^2]$ as N becomes large. This expression is useful even for moderate values of N (e.g. 19). It shows that for a fixed radial occupancy factor η the normalized free energy becomes lower with increasingly fine subdivision. (In a heavy ion fusion (HIF) combiner with a practical lower limit to the beamlet spacing, this could not be continued indefinitely, of course.) In terms of the number M of rings of beamlets, $U_n \sim M^{-2}$ for large M, the same proportionality as for the case of M sheet beams [6].

Square arrays (Section 4), sometimes proposed for HIF, have configurational free energy which is shown to limit the effect of subdivision and prevent $1/N$ scaling. In Section 5 we point out that if a square format is mandated in a large array (e.g. 5×5), then a significant reduction in emittance growth may be obtained by omitting corner beamlets.

2. Merging identical beamlets

In the practical case where all N beamlets have the same charge per unit length (line charge) λ_0 and radius a_0, Eq. (1) is $a_T^2 = a_0^2 + 2\langle|\boldsymbol{\delta}_i - \boldsymbol{\delta}_c|^2\rangle$, the angle brackets indicating an average over all N beamlets. The value of a_T^2 is independent of the choice of origin and we place the origin at the center of mass:

$$a_T^2 = a_0^2 + 2\langle\delta^2\rangle = a_0^2 + 2\langle x^2 + y^2\rangle \tag{3}$$

We write the total line charge as $N\lambda_0 = \Lambda$ and also rearrange terms, so that Eq. (2) becomes

$$U_f = \frac{\Lambda^2}{4\pi\varepsilon_0}\left[-\frac{N-1}{4N} + \frac{1}{2}\ln\left(\frac{a_T^2}{a_0^2}\right) - \frac{1}{N^2}\sum_j \sum_{i<j} \ln\left(\frac{\delta_{ij}^2}{a_0^2}\right)\right] \tag{4}$$

with the notation

$$\delta_{ij}^2 \equiv (x_i - x_j)^2 + (y_i - y_j)^2$$

Note that both logarithms now have a_0^2 in the denominator, which makes the scaling more obvious. We see from Eqs. (3) and (4) that U_f is invariant to scale, i.e. for a given configuration of beamlets, U_f just depends on the *ratio* of beamlet spacings to beamlet size. Of course, the potential r.m.s. emittance growth will depend on the overall scale.

For emittance growth calculations it is convenient to replace U_f with the normalized free energy U_n, which is obtained by dividing U_f by the self-field energy within a uniform beam with the same r.m.s. radius [7], i.e. $U_n = 4U_f(4\pi\varepsilon_0/\Lambda^2)$. Also, the denominators a_0^2 in (4) can be written separately and combined, giving the form used for calculations and for further analysis (see Appendix A):

$$U_n = \frac{4}{N}\left(-\frac{N-1}{4} - \ln a_0 + \frac{N}{2}\ln a_T^2 - \frac{1}{N}\sum_j \sum_{i<j} \ln \delta_{ij}^2\right) \tag{5}$$

(Note that U_n, like U_f, is invariant to scale; the units are irrelevant. U_n is also *independent of the total current.*) These equations do not require the arrangement of beamlets to possess any symmetry or regularity, as long as the beamlets do not overlap. In practice a regular arrangement is chosen, as in the following sections.

2.1. Emittance growth

We define r.m.s. emittance by $\epsilon_x^2 \equiv X^2(V_x^2 - X'^2)$, where X and V_x are r.m.s. values of position and velocity respectively. As in Ref. [3], we assume $X' = 0$ and write $\epsilon = XV_x$. The emittance of a single beamlet before merging is $\epsilon_{x1} = X_1 V_x$ and the initial emittance of the whole array is given by $\epsilon_{xi}^2 = \epsilon_{x1}^2 + \langle \delta_x^2 \rangle V_x^2 = (X_1^2 + \langle \delta_x^2 \rangle) V_x^2$; there is a corresponding equation for y. The subsequent emittance growth for a general non-symmetric beam system has been recently analyzed [7]. For the special case where the initial composite beam is matched, centered and properly aimed, the final (asymptotic) emittance is

$$\epsilon_{xf}^2 = \epsilon_{yf}^2 = \frac{1}{4}\epsilon_{xi}^2\left(1 + \frac{Y_i^2}{X_i^2}\right) + \frac{1}{4}\epsilon_{yi}^2\left(1 + \frac{X_i^2}{Y_i^2}\right) + \frac{Q}{16}(X_i^2 + Y_i^2)U_n + \cdots \quad (6)$$

with higher-order terms neglected. In the special case $V_x = V_y$,

$$\frac{\epsilon_{xf}^2}{\epsilon_{xi}^2} = \frac{X_i^2 + Y_i^2}{2X_i^2}\left(1 + \frac{Q}{8}\frac{U_n}{V_x^2}\right) + \cdots, \quad (6a)$$

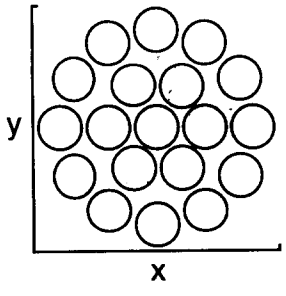

Fig. 1. Array with two rings around a central beamlet; $N = 19$. At maximum non-overlapping diameter, most beamlets are in contact with others.

and similarly for y. Q is the total perveance $2\Lambda q/(4\pi\varepsilon_0 m v_z^2)$. The neglected terms are second order in U_n and also involve the radii of the equivalent elliptical matched beam [7]. From Eq. (3), $X_i^2 + Y_i^2 = a_1^2/2 = \langle \delta^2 \rangle + \frac{1}{2}a_0^2$. Note that the U_n term dominates if the initial beamlets are cool, as in many HIF designs. We calculate U_n for particular array shapes in the following sections and provide further discussion of emittance growth in Section 4.

3. Analytic and calculated results for circular array of beamlets

We use Eq. (5) to investigate the variation in U_n with N for beamlet arrays of various shapes. We start with circular arrays, proposed for large-scale magnetic fusion energy applications [5]. A prototype with 19 beamlets (in a quasi-circular array) was successfully tested at LBNL [5]. Among various shapes, circular arrays have the lowest configurational free energy [7]. In fact, an array of rings in which the number of beamlets per ring is proportional to the radius behaves in the large-N fixed-η limit somewhat like a single beam of uniform particle density, with $U_n = 0$ by definition.

Such an array, with uniform center-to-center ring spacing Δ_r, is illustrated in Fig. 1. The beamlets will not overlap if $0 < a_0 < \Delta_r/2$. The number of beamlets per ring is proportional to the ring radius. For maximum azimuthal density of beamlets the proportionality factor would be 2π, but for simplicity we use the factor 6. (There is no distinction for $N < 91$.) In model shown in Fig. 1, the number of beamlets N, including the central beamlet, is related to the number of rings M by

$$N = 1 + 3M(M+1) \quad (7)$$

For convenience we introduce the occupancy factor η, defined as the ratio of the actual beamlet radius to the maximum radius without overlapping:

$$\eta = \frac{2a_0}{\Delta_r} \quad (0 < \eta < 1) \quad (8)$$

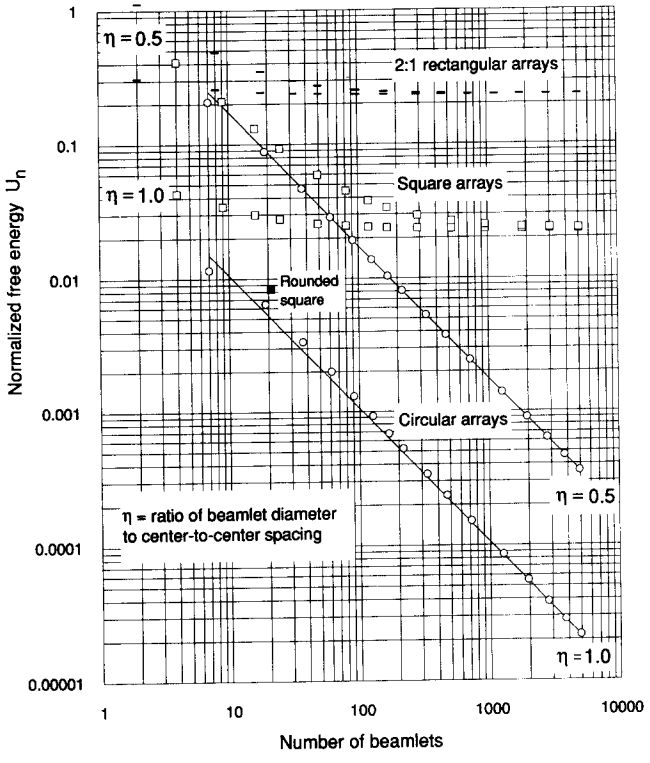

Fig. 2. Normalized free energy vs. N from Eq. (5), showing asymptotic behavior. Full lines are from Eq. (9). See also Tables 1, 3 and 4.

Then, using (7) and (8), we can derive from Eq. (5) our analytical result for large N (see Appendix A):

$$U_n \to \frac{4}{N}\left(\frac{3}{4} - \ln 3 - \ln \eta + \frac{3}{8}\eta^2\right) \tag{9}$$

Fig. 2 plots Eq. (9) as full lines for the cases $\eta = 0.5$ and 1.0. Also plotted are direct calculations from Eq. (5), listed in Table 1. The total number of beamlets ranges from seven to 4921, with N extended beyond the range of practical interest (see caveat in Section 2) to show how the results of (5) approach the asymptotic results of (9). This approach is indicated both in Fig. 2 and in the NU_n columns in Table 1, where the values tend toward the limits 0.1056 and 1.7531 obtained from (9).

From (7) and (9), $U_n \sim 1/M^2$ for large M. It is interesting to compare the sheet beam case, where instead of rings of beamlets one has continuous sheets of current. For M current sheets with initial widths equal to the gaps, i.e. $\eta = 0.5$, we found [6]

$$U_n \text{ (sheet beams)} = 2 - \frac{2}{M}\frac{2M^2 - 1}{(4M^2 - 3)^{1/2}} \tag{10}$$

and it turns out that for $M > 3$, to good accuracy, $U_n = 1/(4M^2)$. See Table 2.

It is not surprising that both cases have the same large-M proportionality. A circular array of round beamlets can expand radially inward and outward, releasing free electrostatic energy in the same way as in the sheet beam case. (The individual beamlets also expand azimuthally, which helps to make the emittance growth isotropic.)

4. Square arrays of beamlets

Square arrays (4×4) have been proposed for HIF accelerator experiments [8]. However, square arrays produce what we call "configurational emittance growth" because their shape does not minimize the normalized free energy U_n for a given number of beamlets. Increasing the number of beamlets for fixed η would give limited im-

Table 1
U_n from Eq. (5) and NU_n vs. total number of beamlets for sets of circular arrays

Rings M	Beamlets N	U_n $\eta = 1.0$	NU_n $\eta = 1.0$	U_n $\eta = 0.5$	NU_n $\eta = 0.5$
1	7	0.011602	0.0812	0.207041	1.4493
2	19	0.006445	0.1224	0.088158	1.6750
3	37	0.003357	0.1242	0.046597	1.7241
4	61	0.001993	0.1216	0.028533	1.7405
5	91	0.001306	0.1189	0.019201	1.7473
6	127	0.000918	0.1166	0.013784	1.7506
7	169	0.000680	0.1149	0.010368	1.7522
8	217	0.000523	0.1135	0.008079	1.7531
10	331	0.000337	0.1115	0.005299	1.7539
12	469	0.000235	0.1102	0.003740	1.7541
15	721	0.000151	0.1089	0.002433	1.7541
20	1261	0.000085	0.1078	0.001391	1.7540
25	1951	0.000055	0.1071	0.000899	1.7538
30	2791	0.000038	0.1067	0.000628	1.7537
35	3781	0.000028	0.1065	0.000464	1.7536
40	4921	0.000022	1.1063	0.000356	1.7535

provement in U_n, because U_n asymptotically approaches a value obtained by integration over a uniform square distribution of space charge. This is seen in Table 3 and Fig. 2, where U_n was calculated from Eq. (5). The subdivision has been extended to large numbers to show that U_n is asymptotically independent of N or η, depending only on the overall shape.

4.1. Emittance growth in square vs. round arrays

For square arrays, Eq. (6a) gives the ratio of final to initial emittance. Here we calculate the initial emittance, normalized with respect to a single *unified* round beam with the same mean square thermal velocity and current density as the individual beamlets and the same total current as all N beamlets. The unified beam radius a_u is given by $a_u^2 = Na_0^2$ and its emittance by $\epsilon_{xu}^2 = Na_0^2V_x^2/4$. From Section 2 the initial emittance is given by $\epsilon_{xi}^2 = (a_0^2/4 + \langle\delta_x^2\rangle)V_x^2$; $\langle\delta_x^2\rangle$ is easily calculated for a square $M \times M$ array: $\langle\delta_x^2\rangle = (M^2-1)a_0^2/3\eta^2$. From these relationships we get

$$\frac{\epsilon_{xi}^2}{\epsilon_{xu}^2} = \frac{N-1}{N}\frac{4}{3\eta^2} + \frac{1}{N} \quad \text{with } N = M^2,\ N \geqslant 4 \qquad (11)$$

Table 2
U_n and M^2U_n vs. number M of rings or sheet beam segments; $\eta = 0.5$

M	U_n(beamlets)	M^2U_n	U_n(sheets)	M^2U_n
2	0.088158	0.353	0.05855	0.2342
3	0.046597	0.419	0.02712	0.2441
5	0.019201	0.480	0.00992	0.2480
10	0.005299	0.530	0.00250	0.2495
20	0.001391	0.556	0.00062	0.2499
30	0.000628	0.566	0.00028	0.2499
40	0.000356	0.570	0.00016	0.2500

Table 3
U_n vs. number of beamlets N in square array, with N extended to show asymptotic behavior

N_x	N_y	N	U_n, $\eta = 1$	U_n, $\eta = 0.5$
2	2	4	0.04286	0.41097
3	3	9	0.03427	0.20944
4	4	16	0.02992	0.13047
5	5	25	0.02765	0.09257
7	7	49	0.02552	0.05889
9	9	81	0.02460	0.04485
11	11	121	0.02412	0.03770
13	13	169	0.02384	0.03357
17	17	289	0.02355	0.02924
23	23	529	0.02336	0.02647
31	31	961	0.02325	0.02496
43	42	1849	0.02319	0.02408
55	55	3025	0.02316	0.02371
71	71	5041	0.02315	0.02347

For round arrays of M rings we have a similar result:

$$\frac{\epsilon_{ri}^2}{\epsilon_{ru}^2} = \left(\frac{N-1}{N}\right)^2 \frac{4}{3\eta^2} + \frac{1}{N}$$

$$\text{with } N = 1 + 3M(M+1),\ N \geqslant 7 \qquad (12)$$

In (12), $\epsilon_r^2 \equiv \epsilon_x^2 + \epsilon_y^2$ and the central beamlet is not counted as a ring. Eqs. (11) and (12) show that if the occupancy η is reasonably close to unity, the initial emittance ratio as defined above is fairly insensitive to the number of rows or rings. A simplified model is

$$\frac{\epsilon_i}{\epsilon_u} \sim \frac{1.15}{\eta} \qquad (13)$$

Eqs. (6a) and (13) may be used to analyze the effect of combining a given set of beamlets or of subdividing a given current into a convenient number of units. In the case of subdivision there are practical restrictions to keep in mind. As mentioned in Section 1 it may be difficult to maintain η if the beamlet sizes become too small. There is also a problem with the current density: smaller beamlets have a larger correction for emittance pressure, so that as N becomes large, the current density tends to be reduced. However, with the low temperature sources used in many HIF designs, the above constant-current-density model works well for N up to around 100. Therefore we will use (13) in the following discussion.

Let us assume that a given total current with a given radius is to be accelerated in one channel of the main accelerator and that this current is so large that it is necessary to divide it among at least four preaccelerator channels. With square or round arrays we have approximately

$$\frac{\epsilon_f}{\epsilon_u} \sim \frac{1.15}{\eta}\left(1 + \frac{Q}{8}\frac{U_n}{V_x^2}\right)^{1/2} \qquad (14)$$

With our cool initial beam assumption (strong tune depression) the U_n term dominates in Eq. (14) and $\epsilon_f \sim U_n^{1/2}$.

Fig. 2 shows the influence of the radial packing fraction η on U_n. With square arrays, U_n falls off rapidly from the 2×2 value as N increases for the case $\eta = 0.5$ but not for $\eta = 1.0$. With $\eta = 0.5$ a 3×3 array cuts U_n in half according to Table 3; the same result could be obtained with only seven beamlets in a circular (hexagonal) array—see Table 1. A 4×4 square array has about one-quarter the normalized free energy of the 2×2 array and the maximum emittance growth is cut in half.

Table 4
U_n vs. number of beamlets N in rectangular array with 2:1 ratio

N_x	N_y	N	U_n, $\eta = 1$	U_n, $\eta = 0.5$
2	1	2	0.31093	1.12186
4	2	8	0.25754	0.48527
6	3	18	0.24420	0.34702
8	4	32	0.23921	0.29735
10	5	50	0.23683	0.27413
14	7	98	0.23472	0.25379
18	9	162	0.23384	0.24539
24	12	288	0.23325	0.23974
30	15	450	0.23297	0.23713
38	19	722	0.23278	0.23538
48	24	1152	0.23267	0.23429
60	30	1800	0.23260	0.23364
76	38	2888	0.23255	0.23320
100	50	5000	0.23252	0.23289

It is more important to achieve large occupancy: if $\eta \to 1$, U_n is reduced by a factor of 10 for the 2×2 case. With $\eta \sim 1.0$ there is little further improvement from subdividing into 3×3 or 4×4 arrays, because the square shape dominates the free energy. However, the seven-beamlet hexagonal shape would reduce U_n by an additional factor of 4.

Other scenarios exist. For example, one might suppose that the preaccelerated beamlets have predetermined currents and radii, so that the merged beam parameters vary with the number of beamlets. Alternatively, one might consider additional mergings after further acceleration. There is not enough space here to discuss all these possibilities.

5. Other shapes of arrays

5.1. Rectangular array

Fig. 2 includes the case of rectangular arrays with a 2:1 ratio, from data shown in Table 4. This configuration has asymptotic normalized free energy about 10 times larger than for the square

configuration, so that there is almost no benefit from subdividing or from increasing η. A wide, thin array could be merged without much emittance growth by using a type of focusing that maintains a ribbon shape, but this would not be feasible for inertial fusion.

5.2. Square array with rounded corners

The ideal ring-type configuration of Section 3 is feasible for MFE sources and preaccelerators [5], but probably not for HIF where merging is done with septums, tending to produce square arrays. In such cases, omitting corner beamlets can be advantageous. For example, a 5×5 array with ideally thin septums ($\eta \to 1.0$) would decrease its U_n by a factor of 3.3 with the elimination of four beamlets. This case is included in Fig. 2, where removing the corners is seen to lower U_n almost to the circular array region.

It may be noted that, besides the major reduction of emittance from decreasing U_n, there is also a minor reduction from the change in radius due to two nearly cancelling effects. The mean square radius must be *increased* by a factor 25/21 to keep the total current constant with fixed current density, while it is *decreased* by a factor 17/21 by the elimination of the corner beamlets. The net effect is to reduce $X_i^2 + Y_i^2$ by a factor of 0.96, influencing both the initial composite emittance and the asymptotic emittance. However, this is insignificant compared with the 0.30 U_n factor which affects $\epsilon_{xf}^2 - \epsilon_{xi}^2$.

Acknowledgements

I thank Edward Lee for discussions that inspired this paper and for additional comments and criticisms which greatly improved it. I also thank Christine Celata for valuable suggestions. This work was supported in part by US DOE Contract DE-AC03-76SF00098.

Appendix A

Here we derive Eq. (9), which gives the normalized free energy U_n for a round array of beamlets arranged as in Fig. 1. We consider Eq. (5) term by term.

Term 1

Using Eq. (7), we have

$$-\frac{N-1}{4} = -\frac{3}{4}M^2 - \frac{3}{4}M \tag{A1}$$

Term 2

As noted under Eq. (5), U_n is invariant to scale, so that we can choose ring spacing $\Delta_r = 1$. Then (8) becomes

$$\eta = 2a_0 \tag{A2}$$

and

$$-\ln a_0 = -\ln\left(\frac{\eta}{2}\right) \tag{A3}$$

Term 3

Each ring has radius $\delta_m = m\Delta_r = m$. In our model (Fig. 1) each ring has $6m$ beamlets, so that in (3)

$$2\langle\delta^2\rangle = \frac{2}{N}\sum_{m=1}^{M} 6m \cdot m^2 = \frac{12}{N}\frac{M^2(M+1)^2}{4}$$
$$= \frac{M^2(1+M^{-1})^2}{1+M^{-1}+3^{-1}M^{-2}}$$

using (7).

$$\ln(2\langle\delta^2\rangle) = 2\ln M + 2\left(\frac{1}{M} - \frac{1}{2M^2} + \cdots\right)$$
$$-\left(\frac{1}{M} + \frac{1}{3M^2} - \frac{1}{2M^2} + \cdots\right)$$
$$= 2\ln M + \frac{1}{M} - \frac{5}{6}\frac{1}{M^2} + \cdots$$

From (3), (A2) and (7)

$$\frac{N}{2}\ln a_T^2 = \frac{N}{2}\ln\left(2\langle\delta^2\rangle + \frac{\eta^2}{4}\right)$$
$$= \frac{N}{2}\ln(2\langle\delta^2\rangle) + \frac{N}{2}\ln\left(1 + \frac{\eta^2}{8\langle\delta^2\rangle}\right)$$

$$= N \ln M + \frac{3}{2}M^2\left(1+\frac{1}{M}+\frac{1}{3M^2}\right) \times \frac{1}{M}\left(1-\frac{5}{6}\frac{1}{M}\cdots\right)+\frac{N}{2}\frac{\eta^2}{8\langle\delta^2\rangle}+\cdots$$

$$= N \ln M + \frac{3}{2}M+\frac{1}{4}+\cdots+\frac{3}{8}\eta^2+\cdots \quad \text{(A4)}$$

Term 4

In the double sum we may specify that the beamlet numbers increase with increasing ring radius. Then beamlet j in ring m interacts with the other beamlets $i<j$ of three classes, namely (a) the central beamlet (Fig. 1), (b) other beamlets in the same ring m and (c) beamlets in rings n of smaller radius than m.

$$\sum_j \sum_{i<j} \ln \delta_{ij}^2 = \sum_{m=1}^{M} (\text{sum}_a + \text{sum}_b + \text{sum}_c) \quad \text{(A5)}$$

We now evaluate these three sums.

$$\text{sum}_a = 6m \ln m^2 = 12m \ln m \quad \text{(A6)}$$

$$\text{sum}_b = \sum_j \sum_{i<j} \ln \delta_{ij}^2$$

$$= 6m\frac{1}{2}\sum_{p=1}^{6m-1} \ln m^2\left\{\sin^2\left(\frac{p\pi}{3m}\right)+\left[1-\cos\left(\frac{p\pi}{3m}\right)\right]^2\right\}$$

$$= 6m\sum_{p=1}^{6m-1} \ln m\, 2\sin\left(\frac{p\pi}{6m}\right)$$

$$= 6m\left[(6m-1)\ln m+\ln\prod_{p=1}^{6m-1} 2\sin\left(\frac{p\pi}{6m}\right)\right]$$

With the identity [9]

$$\prod_{r=1}^{s-1} 2\sin\left(\frac{r\pi}{s}\right) = s$$

we have finally

$$\text{sum}_b = 6[(6m^2-m)\ln m + m\ln(6m)] \quad \text{(A7)}$$

Next, using label k for beamlets in ring n and label p for beamlets in m,

$$\text{sum}_c = \sum_{n=1}^{m-1}\sum_{p=1}^{6m}\sum_{k=1}^{6n} \ln \delta_{kp}^2 \quad \text{(A8)}$$

To evaluate this, we observe that the angle differences between beamlets in rings m and n occur in multiples of $2\pi/6mn$ and then twice use the identity [9]

$$\prod_{r=1}^{s}\left[a^2+b^2-2ab\cos\left(\theta+\frac{2r\pi}{s}\right)\right] = a^{2s}+b^{2s}-2a^sb^s\cos(s\theta)$$

We have

$$\sum_{p=1}^{6m}\sum_{k=1}^{6n} \ln \delta_{kp}^2 = 6\sum_{p=1}^{m} \ln \prod_{k=1}^{6n}\left[m^2+n^2-2mn\cos\left(\frac{k\pi}{3n}-\frac{p\pi}{3mn}\right)\right]$$

$$= 6\sum_{p=1}^{m} \ln\left[m^{12n}+n^{12n}-2m^{6n}n^{6n}\cos\left(6n\frac{p\pi}{3mn}\right)\right]$$

$$= 6\ln(m^{6mn}-n^{6mn})^2$$

$$= 72mn\ln m + 12\ln\left[1-\left(\frac{n}{m}\right)^{6mn}\right]$$

which is exact so far. The last term is $-12(n/m)^{6mn}+\cdots = -12[2^{-12}+O(10^{-6})]$ for $m \geqslant 2$. After doing the sum over n from 1 to $m-1$ in (A8), we have

$$\text{sum}_c = 6[6m^2(m-1)\ln m - 2^{-11} - O(10^{-6})] \quad \text{(A9)}$$

for $m \geqslant 2$. Inserting (A6), (A7) and (A9) in (A5), we have for Term 4 of Eq. (5)

$$-\frac{1}{N}\sum_j\sum_{i<j} \ln \delta_{ij}^2 = -\frac{6}{N}\sum_{m=1}^{M}\left[6\left(m^3+\frac{m}{3}\right)\ln m + m\ln 6 - 2^{-11} - \cdots\right]$$

$$= -\left(N-\frac{3}{10N}\right)\ln M + \frac{9}{4}\frac{M^4}{N} - \frac{9}{4}\frac{1}{N} - \frac{N-1}{N}\ln 6 - \frac{6M}{N}2^{-11} + \cdots \quad \text{(A10)}$$

where we used Eq. (7) for the $\ln 6$ term and summed $(m^3+m/3)\ln m$ with the formula [10]

$$\sum_{x=1}^{M} f(x) = \int_{1}^{M} f(x)\,dx + \frac{1}{2}[f(M)+f(1)] + \frac{1}{12}[f'(M)-f'(1)] - \frac{1}{720}[f'''(M)-f'''(1)] + \cdots$$

In the second term of (A10) we find $M^4/N = (M^2/3)(1 - M^{-1} + \frac{2}{3}M^{-2} + \cdots)$, using Eq. (7) again. Then (A10) becomes, in the limit of large M and N,

$$-\frac{1}{N}\sum_{j}\sum_{i<j} \ln \delta_{ij}^2 \rightarrow -N \ln M + \frac{3}{4}M^2 - \frac{3}{4}M + \frac{1}{2} - \ln 6 \qquad \text{(A11)}$$

Adding (A1), (A3), (A4) and (A11) then gives Eq. (9).

References

[1] P.M. Lapostolle, Energy relationships in continuous beams, CERN Rep. CERN-ISR-DI/71-6, 1971; Possible emittance increase through filamentation due to space charge in continuous beams, IEEE Trans Nucl. Sci. NS-18 (1971) 1101.

[2] E.P. Lee, S.S. Yu and W.A. Barletta, Phase space distortion of a heavy-ion beam propagating through a vacuum reactor vessel, Nucl. Fus. 21 (1981) 961.

[3] C.M. Celeta, A. Faltens, D.L. Judd, L. Smith and M.G. Tiefenback, Transverse combining of nonrelativistic beams in a multiple beam induction linac, Proc. 1987 Particle Accelerator Conf., p. 1167; personal communication, 1993.

[4] E.P. Lee, Nonlinear field energy of a set of N beams, Lawrence Berkeley Laboratory Rep. LBL-38317, 1996; personal communication, 1993.

[5] O.A. Anderson, W.S. Cooper, W.B. Kunkel, K.N. Leung, A.F. Lietzke, C.F.A. van Os, L. Soroka, J.W. Stearns and R.P. Wells, Negative ion source and accelerator systems for neutral beam injection in large Tokamaks—Part A, Plasma Physics and Controlled Nuclear Fusion Research 1990, Vol. 3, International Atomic Energy Agency, Vienna, 1991, p. 503; J.W. Kwan et al., Rev. Sci. Instrum. 66 (1995) 3864.

[6] O.A. Anderson, Internal dynamics and emittance growth in space-charge-dominated beams, Part. Accel. 21 (1987) 197.

[7] O.A. Anderson, Emittance growth in non-symmetric beam configurations, Lawrence Berkeley Laboratory Rep. LBL-38852, 1996. Preprint for EPAC 96 (Fifth European Particle Accelerator Conference, Barcelona).

[8] ILSE Conceptual Engineering Design Study, Lawrence Berkeley Laboratory PUB-5219, 1989, p. 35.

[9] Z.A. Melzak, Companion to Concrete Mathematics, Wiley, New York, 1973, p. 99.

[10] H.T. Davis, The Summation of Series, Principia, San Antonio, TX, 1962, p. 49.